In vivo functional connectome of human brainstem nuclei of the ascending arousal, autonomic, and motor systems by high spatial resolution 7-Tesla fMRI

As Published: 10.1007/S10334-016-0546-3

Publisher: Springer Science and Business Media LLC

Persistent URL: https://hdl.handle.net/1721.1/134987

Version: Author's final manuscript: final author's manuscript post peer review, without publisher's formatting or copy editing

HHS Public Access

Author manuscript

MAGMA. Author manuscript; available in PMC 2016 June 03.

Published in final edited form as:

MAGMA. 2016 June ; 29(3): 451–462. doi:10.1007/s10334-016-0546-3.

In vivo functional connectome of human brainstem nuclei of the ascending arousal, autonomic and motor systems by high spatial resolution 7 Tesla fMRI

Marta Bianciardi[1], **Nicola Toschi**[1,2], **Cornelius Eichner**[1], **Jonathan R. Polimeni**[1], **Kawin Setsompop**[1], **Emery N. Brown**[3], **Matti S. Hamalainen**[1], **Bruce R. Rosen**[1], and **Lawrence L. Wald**[1]

[1]Department of Radiology, Athinoula A. Martinos Center for Biomedical Imaging, Massachusetts General Hospital and Harvard Medical School, Bldg. 149, 13th Street, Charlestown, Boston, MA 02129, United States

[2]Medical Physics Section, Department of Biomedicine and Prevention, Faculty of Medicine, University of Rome “Tor Vergata”, Via Montpellier 1, 00133, Rome, Italy

[3]Department of Anesthesia, Critical Care and Pain Medicine, Massachusetts General Hospital, 55 Fruit Street, Boston, MA 02114, United States

Abstract

Object—To map the *in vivo* human functional connectivity of several brainstem nuclei with the rest of the brain by using seed-based correlation of ultra-high magnetic field functional magnetic resonance imaging (fMRI) data.

Materials and Methods—We used the recently developed template of 11 brainstem nuclei derived from multi-contrast structural MRI at 7 Tesla as seed regions to determine their connectivity to the rest of the brain. To achieve this, we utilized the increased contrast-to-noise ratio of 7 Tesla fMRI compared to 3 Tesla and the time efficient simultaneous multi-slice imaging to cover the brain with high spatial resolution (1.1 mm-isotropic nominal resolution) while maintaining a short repetition time (2.5 s).

Results—The delineated Pearson’s correlation-based functional connectivity diagrams (connectomes) of 11 brainstem nuclei of the ascending arousal, motor and autonomic systems from 12 controls are presented and discussed in the context of existing histology and animal work.

Corresponding author: Marta Bianciardi, Athinoula A. Martinos Center for Biomedical Imaging, Department of Radiology, Massachusetts General Hospital, Building 149, Room 2301, 13th Street, Charlestown, MA 02129, USA, Phone: +1 617 724 1723; Fax: +1 617 726 7422, ; Email: martab@nmr.mgh.harvard.edu

Author’s contribution

Drs. Bianciardi, Toschi, Eichner, Polimeni, Setsompop acquired the data. Data analysis was carried out by Dr. Bianciardi and partly by Dr. Toschi. All the authors substantially contributed to the project development, data interpretation, drafted the article and approved the final version to be published.

Conflict of Interest: The authors declare that they have no conflict of interest.

Compliance with Ethical Standards

Ethical Approval: All procedures performed in studies involving human participants were in accordance with the ethical standards of the institutional research committee of the Massachusetts General Hospital and with the 1964 Helsinki declaration and its later amendments or comparable ethical standards.

Informed Consent: Informed consent was obtained from all individual participants included in the study.

Conclusion—Considering that the investigated brainstem nuclei play a crucial role in several vital functions, the delineated preliminary connectomes might prove useful for future *in vivo* research and clinical studies of human brainstem function and pathology, including disorders of consciousness, sleep disorders, autonomic disorders, Parkinson's disease and other motor disorders.

Keywords

In vivo functional connectome; human brainstem nuclei; high spatial resolution; 7 Tesla; simultaneous multi-slice imaging

1. Introduction

The *in vivo* investigation of the functional connectivity of brainstem nuclei (Bn) with other subcortical and cortical regions ("brainstem-brain" connectome) at rest lags far behind the delineation of the resting-state connectomes of other brain regions, such as the cortex and other subcortical areas [1–3]. This is because precise anatomical localization of several of these nuclei by conventional structural neuroimaging has remained elusive. Additionally, a brainstem-brain connectome would simultaneously require high-spatial resolution and whole-brain coverage, a condition usually difficult to be met due to limited sensitivity in deeper parts of the brain and limited speed of conventional fMRI techniques.

An *in vivo* brainstem-brain functional connectome could prove useful as a biomarker of disease, including devastating conditions such as coma and Parkinson's disease. Human gray matter Bn are indeed regulatory centers of vital functions, such as arousal, autonomic homeostasis, sensory and motor relay, cranial nerve function, and nociception; notably, impairment in the regulation of these functions has been associated with disorders of consciousness, sleep disorders, cardiovascular disease, psychiatric disorders, motor disorders, chronic pain, altered autonomic functions [4–10].

The aim of this work was to first demonstrate the feasibility of measuring the resting-state functional connectivity between the brainstem and other brain areas in individuals and to provide an *in vivo* preliminary baseline functional brainstem-brain connectivity diagram (connectome) of the healthy brain, which might be useful for future research and clinical studies of the brainstem in health and disease. To achieve whole-brain coverage, high spatial resolution, non-prohibitively long repetition time (TR) and high fMRI sensitivity required to delineate an *in vivo* brainstem-brain functional connectome, we took advantage of ultra-high field fMRI for brainstem imaging and recent advances in the MRI acquisition speed. First, we focused on the specific Bn of the ascending arousal, autonomic and motor systems which we have recently delineated by the use of multi-contrast distortion- and resolution-matched echo-planar images (EPI) at 7 Tesla [11]. Specifically, we used this original template of Bn labels in standard (Montreal Neurological Institute, MNI) space [11] to define the location of seed regions for hypothesis-driven (i.e. based on the anatomical location of Bn) brainstem-brain fMRI connectivity analysis. Further, in order to exploit the dependence of sensitivity and blood oxygenation level dependent (BOLD) contrast on field strength [12], we acquired ultra-high magnetic field (7 Tesla) resting-state fMRI data with high spatial resolution (1.1

mm isotropic voxels) while accounting for physiologic noise contributions (especially pulsatility effects around the CSF and the vasculature). Finally, we employed the recently developed [13] simultaneous-multi-slice imaging technique to simultaneously acquire three slices at a time, and cover the whole brain (with 123 sagittal slices) with good temporal sampling (TR = 2.5 s), as needed to delineate the brainstem-brain connectome.

2. Material and Methods

2.1 Experimental design

Twelve (6 males, 6 females, mean age ± s.e.: 28 ± 1 years, age range = [20 36]) healthy subjects (the same subjects participating in [11]) underwent 7 Tesla MRI (Siemens Healthcare, Erlangen, Germany), after giving written informed consent. The human subject protocol was approved by the Institutional Review Board of the Massachusetts General Hospital. During the 7 Tesla MRI session, subjects were asked to rest with their eyes closed while laying down in the scanner during image acquisition. Head motion was minimized by the use of foam pads, placed in the space between the interior coating of the MRI detector array and the subject's head. For RF transmission we employed a detunable band-pass birdcage coil, and a custom-built 32-channel radiofrequency loop coil head array was used for reception.

2.2 fMRI data acquisition

We acquired 1.1 mm isotropic gradient-echo EPIs with parameters: matrix size/GRAPPA factor/nominal echo-spacing/readout bandwidth/N. slices/slice orientation/slice acquisition order/echo time (TE)/repetition time (TR)/flip angle (FA)/simultaneous multi slice factor/N. repetitions/phase encoding direction = 180 × 240/3/0.82 ms/357.1 kHz/123/sagittal/interleaved/32 ms/2.5 s/75°/3/210/anterior-posterior. fMRI data were acquired during the same session and with the same spatial resolution, echo-spacing and phase encoding direction as multi-contrast EPI images of [11], used to generate the probabilistic atlas of 11 Bn. To correct for spatial distortions a 2.7 mm isotropic GRE field map was acquired with parameters: matrix size/bandwidth/N. slices/slice orientation/slice acquisition order/TEs/TR/FA = 270 × 270/1515 Hz-per-pixel/70/sagittal/interleaved/[2.79 3.81] ms/570 ms/36°. To aid alignment of EPIs to the MNI T1-weighted template, we also acquired a 1 mm isotropic T1-weighted multi-echo MPRAGE image: TR = 2.51 s; 4 echoes with TEs = [1.6, 3.5, 5.3, 7.2] ms, inversion time = 1.5 s, flip angle = 7°, FOV = 256×256×176 mm^3, 256×256×176 matrix, bandwidth = 651 Hz/pixel, GRAPPA factor = 2, acquisition time: 6′04″. The root-mean-square MPRAGE image across echo-times was computed and the bias field corrected (SPM8, London, UK); to aid the co-registration of EPIs to the MPRAGE, the blood compartments (e.g. arteries) displaying hyperintense signal in the 7 Tesla MPRAGE were identified by thresholding the image at the 95^{th} percentile and successively masked out.

2.3 fMRI data analysis

Preprocessing—For each subject, EPIs were slice-timing (by FMRIB Software Library, FSL4.1, Oxford, UK) and motion (FSL4.1) corrected. The EPIs were then aligned to the MNI space using the following procedure: (i) the EPIs were aligned to the MPRAGE by a white-matter-boundary-based registration (epi_reg, FSL4.1), which also included distortion

correction by the use of the acquired field map; (ii) the non-linear transformation that aligned the MPRAGE to the T1-weighted MNI 152 template (1 mm resolution) was computed (Advanced Normalization Tool, ANTs, Philadelphia, USA) and (iii) applied to the EPIs. The non-linear registration (ii) included a generic affine transformation (computed by concatenating center-of mass alignment, rigid, similarity and fully affine transformations) followed by a high-dimensional non-linear transformation (symmetric diffeomorphic normalization transformation model with neighborhood cross correlation, regular sampling, gradient step size: 0.15, four multi-resolution levels, smoothing sigmas: 3, 2, 1, 0 voxels – fixed image space –, shrink factors: 6, 4, 2, 1 voxels – fixed image space –, histogram matching of images before registration, data winsorization – quantiles: 0.001, 0.999 –, convergence criterion: slope of the normalized energy profile over the last 10 iterations < 10^{-8}); the affine and non-linear transformations were combined into a single warp field to be applied to the EPI (for each data-set the quality of the coregistration is shown in Figure S1). Regions outside the brain were removed (FSL4.1), and no spatial smoothing was applied. Time-courses were then corrected for physiological noise, including the removal of low-frequency signals, e.g. drifts, by high-pass filtering at 0.01 Hz (AFNI, Bethesda, MD, USA), and the removal of the mean time-course in a region containing mainly cerebrospinal fluid (CSF), i.e. a CSF mask [14]. The CSF mask (see also Figure S2) was identified in a 5.3 × 6.5 × 7.5 cm box containing the brainstem by computing the signal standard deviation over time and considering only the voxels with standard deviation above a threshold value (above 55). Crucially the CSF mask (Figure S2) mainly contained voxels in the CSF-spaces neighboring the brainstem, including the forth ventricle and the cerebral aqueduct. Previous work [15] showed that removal of the signal of the cerebral aqueduct is important for the functional connectivity analysis of adjacent brainstem nuclei, such as the periaqueductal gray. Finally, time-courses were low-pass filtered at 0.1 Hz (AFNI).

Region-based correlation analysis—For each subject, we performed a region-based correlation analysis between seed and target regions in MNI space. The 18 structural probabilistic Bn labels (7 bilateral, i.e. left and right, and 4 medial regions, for a total of 11 different Bn) of [11] were employed as seed-regions: 2 subregions (bilateral, i.e. 2 left and 2 right) of the substantia nigra (region 1 compatible with pars reticulata, and region 2 with pars compacta), 2 subregions (bilateral) of the subthalamic nucleus and of the red nucleus, the inferior olivary nucleus (bilateral), the raphe magnus, the median raphe, the dorsal raphe and the periaqueductal gray. Target regions comprised the 18 structural Bn seed regions described above as well as 48 bilateral cortical and 7 bilateral subcortical regions of the Harvard-Oxford atlas [16] (probabilistic labels thresholded at 25 %), 10 bilateral subregions of the cerebellum, and 8 (medial) subregions of the cerebellar vermis [17] (probabilistic labels thresholded at 25 %), for a total of 156 target regions (the region names are listed in Figures 1–3). For each subject, we averaged the time-courses within seed and target regions (or “nodes”) and computed the Pearson correlation coefficient across them, generating an 18 × 156 correlation matrix (with 18 × (18 − 1)/2 + 18 × (156 − 18) = 2637 correlation values above the diagonal). To test for statistical significance, the one sample Student’s *t*-test was performed on correlation values across subjects with the null hypothesis of zero correlation, followed by false discovery rate (FDR) correction for multiple comparisons ($q = 0.05$) across the whole matrix. For each seed region, a connectome of significant correlation

values (which we call “connections” or “links”) at the group level was displayed using a circular 2D representation (Matlab v. 8.4, Natick, MA), similar to the one proposed in [2].

Connectivity metrics—With the aim of evaluating the connectivity of target regions with Bn, for each target region (whole-brain nodes, including Bn themselves) we computed standard connectivity metrics of graph theory [18]: a) the *target-node degree* as the number of links connected from Bn to each target region; b) the *target-node strength* as the sum of the Pearson’s correlation values (“weights”) of links connected to the target region; c) the *target-node mean strength* as the target-node strength divided by the target-node degree. As a measure of the connectivity of seed regions (Bn) to the rest of the brain, for each seed region (Bn) we measured the *seed-node degree* as the number of links originating from Bn to target regions; b) the *seed-node strength* as the sum of the Pearson’s correlation values (“weights”) of links originating from Bn to target regions; c) the *seed-node mean strength* as the seed-node strength divided by the seed-node degree. We also separately computed the *seed-node degree/strength/mean strength towards Bn* (i.e. considering as target regions Bn only), as a measure of the brainstem-brainstem (i.e. local, short distance) connectivity and the *seed-node degree/strength/mean strength towards the rest of the brain* (target regions outside the brainstem), which measures the brainstem-brain (i.e. distal, long range) connectivity.

Preliminary validation of the probabilistic Bn atlas use—Variability in individual brainstem anatomy (due to residual misalignment of single subject EPIs to the probabilistic Bn atlas space and/or variability in the Bn shape, size and location) may have introduced bias in the connectivity results, and hence prevented a valid use of the probabilistic Bn atlas. To verify if this was the case, we used single-subject Bn labels [11] as seed regions for the connectivity analysis, rather than probabilistic Bn labels [11]. Single-subject Bn labels were delineated in [11] using multi-contrast anatomical EPIs acquired in the same subjects, during the same session and with the same spatial resolution and geometric distortion as the functional EPIs of this work. We co-registered single-subject Bn labels to MNI-space using non-linear transformations, and computed the correlation matrix of the 18 seed Bn labels with 156 target regions, as above.

Variability across the population—we assessed the variability of the connectivity results across the population by computing the coefficient of variation of the correlation matrix across subjects. We also assessed possible gender difference of the connectivity results by computing the similarity (correlation) between the correlation matrix averaged across male participants and the correlation matrix averaged across female subjects.

3 Results and Discussion

In the following sections we present the estimated connectomes and compared them to expected connectivity pathways derived from prior work. We then summarize the properties of local (brainstem-brainstem) and distal (brainstem-brain) Bn connectivity, emerging from the analysis of basic connectivity metrics based on graph theory. Moreover, we show the validity of using the probabilistic Bn atlas to delineate the Bn connectome in fMRI data precisely coregistered to MNI space, and assess the variability of the connectivity results across subjects. Further, we discuss the employed seed-based functional connectivity

approach with respect to other approaches, and evaluate the limitations of this work. Finally, we emphasize the potential of the developed connectome as a preliminary connectivity profile, which might prove useful for future clinical and research work.

3.1 Connectome of Bn of the motor network

In Figure 1 we show the region-based functional connectome at the group level of the left red nucleus–subregion 1, left red nucleus–subregion 2, and left inferior olivary nucleus, which pertain to the motor system. Similar results were obtained for the right inferior olivary nucleus, right red nucleus–subregion 1 and right red nucleus–subregion2 (for each region, the similarity between the correlation values of left and right nuclei was significant at $p < 0.0002$).

The *red nucleus subregion 1* displayed significant connectivity with other Bn of the motor system (inferior olivary nuclei, red nucleus-subregion 2, and the two subregions of subthalamic nuclei and of the substantia nigra), with the cerebellum, fronto-orbital and insular regions, areas of the limbic system (e.g. anterior division of the cingulated gyrus, paracingulate and parahippocampal gyri, hippocampus), with basal ganglia (thalamus, caudate, putamen, pallidum), and precuneus among other regions, in agreement with previous work [19–20]. Nevertheless, the subregion 1 (nor subregion 2) of the red nucleus did not connect with the inferior olivary nuclei, in spite of their structural connection via the rubro-olivary tract [19]. Interestingly, the connectivity of the *subregion 2 of the red nucleus* only partially overlapped with that of subregion 1, with a marked decrease in connectivity with several cerebellar regions in the former compared to the latter, and with a significant connectivity with cortical motor areas (absent for subregion 1), such as the precentral gyrus and the supplementary motor cortex (which in the Harvard-Oxford atlas is called juxtapositional lobule cortex).

The connectivity of the *inferior olivary nucleus* was very dense and included most of the cerebellum, motor regions (the precentral gyrus and the juxtapositional lobule cortex), putamen and pallidum, as expected from previous work [21] as well as limbic areas, temporal and occipital regions among others.

The region-based connectomes at the group level of the left substantia nigra–subregion 1 and –subregion 2, left subthalamic nucleus–subregion 1 and –subregion 2 is shown in Figure 2. Similar results were obtained for the right substantia nigra–subregions and subthalamic–subregions (for each region, the similarity between the correlation values of left and right nuclei was significant at $p < 0.0002$).

Our results show that the *two subregions of substantia nigra and of subthalamic nucleus* were strongly connected to each other, to the thalamus, dorsal striatum (caudate, putamen), ventral striatum (accumbens), pallidum, motor cortex (pre-central gyrus and juxtapositional lobule), nodes of the default mode network (such as the precuneous and posterior cingulate), frontal areas (e.g. frontal pole, superior and middle frontal gyrus), cerebellum (e.g. strongly with cerebellum vermis VI), and limbic regions (e.g. anterior cingulated and paracingulate areas, hippocampus). This is in line with previous *ex vivo* work and *in vivo* structural connectivity work demonstrating the existence of these connectivity pathways of the motor

basal-ganglia system (see [22–25] for the SN and [26–27] for STh). Interestingly, both subregions of the subthalamic nucleus (and not exclusively one or the other subregion) identified in [11] were functionally connected to both limbic and motor areas, in contrast with the existence in primates of spatially distinct limbic and motor (as well as associative) zones of the subthalamic nucleus [26–27]. Further, the two subregions of the substantia nigra [11] did not display a strong preferential connectivity pattern towards either the dorsal or the ventral striatum, as showed for previous subdivisions of the substantia nigra [22,25]; this finding might be related either to the polysynaptic nature of the generated Pearson's correlation-based connectome or to the location of the two subregions within the substantia nigra.

3.2 Connectome of Bn of the ascending arousal and autonomic networks

The region-based connectome at the group level of the median raphe, dorsal raphe, raphe magnus and periaqueductal gray, which pertain to the ascending arousal and autonomic networks, is shown in Figure 3.

Our results show that Bn of the arousal system, such as the *median raphe*, displayed significant connectivity with the thalamus, basal forebrain (e.g accumbens), other brainstem nuclei of the arousal/autonomic system (e.g. dorsal raphe, PAG), limbic regions (paracingulate gyrus, anterior division of the cingulated gyrus, cerebellum VI—part of the salience network [28–29]—and the hippocampus) as expected from previous work [4–5, 30–32]. The MnR also displayed significant functional connectivity with regions belonging to the default mode network [29,33] (precuneous, posterior division of the cingulated gyrus, anterior and posterior divisions of the middle temporal gyrus, thalamus, hippocampus, cerebellum crus IX), and to the executive network [29,34–35] (frontal pole, cerebellum Crus I, Crus II, III), and basal ganglia (putamen, thalamus), among other areas. Interestingly, the connectivity pathways of the median raphe (e.g. with the anterior cingulate, thalamus, basal ganglia, cerebellum) partially overlapped with those delineated in recent fMRI work [36], based on the identification of the location of the median and dorsal raphe by serotonin transporter PET imaging performed on the same subjects undergoing fMRI.

The connectome of the *dorsal raphe* was very sparse (significant connectivity only with the periaqueductal gray, median raphe and right cerebellum crus IX), as opposed to the widespread connectivity pathways expected from previous work in rats (e.g. with the thalamus, midbrain, amygdala, dorsal and ventral striatum, basal forebrain, lateral hypothalamus and several cortical regions [31–32]).

The *periaqueductal gray* displayed strong connectivity with the thalamus, accumbens, cerebellum, executive network (frontal pole, cerebellum Crus I, Crus II, III) and some limbic regions of the salience network (paracingulate gyrus, anterior division of the cingulated gyrus, cerebellum VI), as expected from previous work [8,37], yet the connectivity with the amygdala and the raphe magnus was not significant. It also displayed strong connectivity with the basal ganglia (caudate putamen, pallidum), default mode network (precuneus, posterior cingulated gyrus, cerebellum VI), and other brainstem nuclei such as the dorsal and median raphe, red nucleus subregion 1 and substantia nigra subregion 1.

Interestingly, the *raphe magnus* displayed significant (yet sparse) connectivity with motor regions (e.g. the neighboring inferior olivary nuclei and several lateral and medial cerebellar regions), as expected for this autonomic motor nucleus [38], which senses changes in the internal and external environment, and modulates the motor output to maintain homeostasis.

3.3 Connectivity metrics of the brainstem-brain connectome

Results of graph-based analysis of connectivity metrics are displayed in Figure 4. Graph-theory-based analysis of connectivity metrics showed that 46% of brain regions were target hubs of Bn (i.e. brain regions that displayed the highest —and above the average— connectivity degree with the investigated Bn), including the thalamus, limbic regions (e.g. paracingulate gyrus, anterior division of cingulated gyrus), regions of the default mode network (e.g. precuneous, posterior division of the cingulated gyrus), regions of the executive network (such as the frontal pole, superior frontal gyrus), several cerebellar regions (e.g. Vermis VIIa, Vermis IX, I–IV), the basal ganglia (putamen, caudate, accumbens), motor cortices (precentral gyrus, juxtapositional lobule) and sensory regions (Heschl's gyrus, lateral-occipital cortex, post-central gyrus). Among Bn, midbrain nuclei (i.e. the two subregions of the substantia nigra, red nucleus and subthalamic nucleus), followed by the periaqueductal gray and median raphe were the target Bn with the highest connectivity with other Bn.

Interestingly, as seed regions, the inferior olivary nuclei (followed by the red nucleus–subregion 1) displayed the highest brainstem-brain distal connectivity, yet exhibited a low local (brainstem-brainstem) connectivity. Further, the two subregions of the substantia nigra had the highest local connectivity and moderately high distal connectivity, while the periaqueductal gray had intermediate both local and distal connectivity.

3.4 Preliminary validation of the probabilistic Bn atlas use

For each Bn label, the connectivity results obtained with the probabilistic Bn labels showed a high degree of similarity with respect to those obtained using single-subject labels ($p < 0.05 \cdot 10^{-34}$), see Figure S3. This may indicate low variability in individual brainstem anatomy (for instance due to residual misalignment of single subject EPIs to the probabilistic Bn atlas space and/or variation in the Bn shape, size and location). Thus, this comparison provided a preliminary validation of the use of the probabilistic Bn atlas to automatically identify the location of Bn in fMRI data precisely co-registered to MNI (i.e. the Bn atlas) space.

3.5 Variability of the connectivity values across subjects

To provide the range of variability of the connectivity results across the population, the coefficient of variation of correlation values (mean ± s.e. across significant correlation values, q = 0.05 FDR corrected) for each Bn is shown in supplementary Figure S4. The dorsal raphe, periaqueductal gray and raphe magnus displayed the highest variability across subjects, the midbrain nuclei and the median raphe the lowest. A high degree of similarity was observed between the correlation matrix averaged across male participants and the correlation matrix averaged across female participants ($r = 0.7$, $p < 10\text{^}-5$), indicating low variability of the connectivity results across gender.

3.6 Methodological strengths and limitations

Our current knowledge of brainstem structural and functional connectivity pathways largely derives from prior (non-human) animal and *ex vivo* work [7–8,22–26,30–32,37–39]. Several factors have hindered the development of an *in vivo* functional brainstem-brain connectome, most of all the difficulty of precisely localizing Bn in neuroimages of living subjects, as well as the demanding fMRI acquisition requirements to map these pathways: high sensitivity, high spatio-temporal resolution, and whole-brain coverage—including the brainstem. The preliminary functional *in vivo* brainstem-brain connectome developed here was obtained by overcoming these technological limitations by using a 7 Tesla scanner and simultaneous-multi-slice imaging, as well as by building upon a recently developed Bn template in MNI space [11], which aided the automatic localization of Bn in our fMRI co-registered to MNI space. This approach enabled the construction of a hypothesis-driven connectome, i.e. a connectome based on the a-priori anatomical knowledge of the Bn location [11], as opposed to previous work [40–41], which employed a data-driven independent-component-analysis-based identification of functionally connected brainstem regions. The generated connectome and its interpretation strictly depend on the parcellation method employed: first, because the functional parcellation of brainstem regions provided by data-driven methods such as independent component analysis might not fully spatially overlap with the structural probabilistic Bn atlas employed in this work (see [42] for our preliminary comparison of the two methods, showing on average across Bn a spatial overlap between the two methods of ~ 40 %); second, because the adopted region-based correlation approach evaluates only the correlation of the averaged time-courses of seed and target regions, and does not capture the variability of the signals across voxels within each region, resulting in possible information loss, as opposed to data-driven whole-brain voxelwise clustering approaches [43] as well as to data-driven methods based on independent component analysis [44].

Methodological limitations of Pearson's correlation-based functional connectivity might confound the interpretation of the connectomes of Bn. For instance, functional connectivity based on the Pearson's correlation coefficient might detect spurious indirect connections (two regions might be indirectly correlated because each of them correlates to a third region or because of the presence of a common source of fluctuations—for instance systemic physiological noise or large draining vein effects), thus confounding the interpretation of the obtained functional connectome. Spurious indirect connectivity might especially confound the connectivity pathways of spatially neighboring Bn (such as for instance the two subregions of the substantia nigra, subthalamic nucleus, red nucleus, or the raphe magnus and neighboring inferior olivary nuclei). To tackle these possible confounds of Pearson's correlation-based functional connectivity future work will investigate the functional connectivity of Bn by other methods, for instance partial-correlation analysis [45], which takes into account spurious correlations, yet at the expense of some sensitivity (thus requiring longer scan times), as well as by the use of more comprehensive physiological noise models [46].

The Bn connectome was developed for a young adult population. Considering that the functional connectivity of Bn might vary with maturation and aging processes, care should

be taken when translating the knowledge derived from this connectome to different age cohorts, including children and older adults.

3.7 On the use of the developed *in vivo* brainstem-brain functional connectome

The developed preliminary Bn connectome brings new pieces of information to the complex *in vivo* wiring diagram of the brain [1–3, 47–48], and we foresee that it might advance our understanding of *in vivo* arousal, autonomic and motor mechanisms in health from a network level perspective. Crucially, if further developed and characterized, it might also facilitate the detection of which specific Bn pathways are impaired at the single-subject level in patients with brainstem structural and functional pathologies (e.g. disorders of consciousness, sleep disorders, chronic pain, cardiovascular disease, Parkinson's disease [4–10, 49–51]). Connectomes have been used in previous work to assess the consequence of and monitor the progression of recovery from network-level brain damage due to traumatic brain injury [52–53], as well as to assess brain development [54].

4. Conclusion

The brainstem plays an important role in several vital functions, e.g. arousal, autonomic function, motor control, nociception [30]. Consequently, mapping the brainstem connectome is important for both the understanding of normal brain function in these domains and associated pathologies [4–10]. However, the complex wiring diagram of the *in vivo* human brainstem-brain connectivity pathways is under-developed compared to that of the rest of the brain, e.g. cortex and other subcortical regions, such as the thalamus and the striatum [1–3, 47–48]. In this work we built a preliminary functional map of the connections of 11 Bn with the rest of the brain in healthy young adults. This connectome, although preliminary in nature because of the inclusion of relatively few Bn (only 11 compared to more than 100 Bn identified *ex vivo* [30,55–56], is a stepping stone towards a more comprehensive understanding of the brainstem functional connectivity in humans. This work extends the ambitious efforts of the Human Connectome projects [3,57], aimed at charting the complex wiring diagram of the human healthy brain by the use of a combination of imaging technologies and existing brain atlases [58–60]. Our work demonstrates the feasibility of mapping functional connectivity between Bn [11] and other brain areas in individual subjects, and of delineating a group connectome of these nuclei. We hope the developed connectome of Bn of the ascending arousal, autonomic and motor systems may pave the way for future studies of brainstem circuitry in pathologies that entail disruption of the pathways of these functional domains [4–10].

Supplementary Material

Refer to Web version on PubMed Central for supplementary material.

Acknowledgments

This work was supported by these sources of funding: NIH NIBIB P41-RR014075, NIH NCRR S10-RR023043 and S10-RR023401.

References

1. Achard S, Salvador R, Whitcher B, Suckling J, Bullmore E. A resilient, low-frequency, small-world human brain functional network with highly connected association cortical hubs. J Neurosci. 2006; 26:63–72. [PubMed: 16399673]
2. Irimia A, Chambers MC, Torgerson CM, Van Horn JD. Circular representation of human cortical networks for subject and population-level connectomic visualization. Neuroimage. 2012; 60:1340–1351. [PubMed: 22305988]
3. Smith SM, Vidaurre D, Beckmann CF, Glasser MF, Jenkinson M, Miller KL, Nichols TE, Robinson EC, Salimi-Khorshidi G, Woolrich MW, Barch DM, Ugurbil K, Van Essen DC. Functional connectomics from resting-state fMRI. Trends Cogn Sci. 2013; 17:666–682. [PubMed: 24238796]
4. Brown EN, Lydic R, Schiff ND. General anesthesia, sleep, and coma. N Engl J Med. 2010; 363:2638–2650. [PubMed: 21190458]
5. Edlow BL, Haynes RL, Takahashi E, Klein JP, Cummings P, Benner T, Greer DM, Greenberg SM, Wu O, Kinney HC, Folkerth RD. Disconnection of the ascending arousal system in traumatic coma. J Neuropathol Exp Neurol. 2013; 72:505–523. [PubMed: 23656993]
6. Hanihara T, Amano N, Takahashi T, Itoh Y, Yagishita S. Hypertrophy of the inferior olivary nucleus in patients with progressive supranuclear palsy. Eur Neurol. 1998; 39:97–102. [PubMed: 9520070]
7. Kinney HC, Richerson GB, Dymecki SM, Darnall RA, Nattie EE. The brainstem and serotonin in the sudden infant death syndrome. Annu Rev Pathol. 2009; 4:517–550. [PubMed: 19400695]
8. Linnman C, Moulton EA, Barmettler G, Becerra L, Borsook D. Neuroimaging of the periaqueductal gray: state of the field. Neuroimage. 2012; 60:505–522. [PubMed: 22197740]
9. Samii A, Nutt JG, Ransom BR. Parkinson's disease. Lancet. 2004; 363:1783–1793. [PubMed: 15172778]
10. Saper CB, Fuller PM, Pedersen NP, Lu J, Scammell TE. Sleep state switching. Neuron. 2010; 68:1023–1042. [PubMed: 21172606]
11. Bianciardi M, Toschi N, Edlow BL, Eichner C, Setsompop K, Polimeni JR, Brown EN, Kinney HC, Rosen BR, Wald LL. Toward an In Vivo Neuroimaging Template of Human Brainstem Nuclei of the Ascending Arousal, Autonomic, and Motor Systems. Brain Connect. 2015; doi: 10.1089/brain.2015.0347
12. Duyn JH. The future of ultra-high field MRI and fMRI for study of the human brain. Neuroimage. 2012; 62:1241–1248. [PubMed: 22063093]
13. Setsompop K, Gagoski BA, Polimeni JR, Witzel T, Wedeen VJ, Wald LL. Blipped-controlled aliasing in parallel imaging for simultaneous multislice echo planar imaging with reduced g-factor penalty. Magn Reson Med. 2012; 67:1210–1224. [PubMed: 21858868]
14. Jo HJ, Saad ZS, Simmons WK, Milbury LA, Cox RW. Mapping sources of correlation in resting state FMRI, with artifact detection and removal. Neuroimage. 2010; 52:571–582. [PubMed: 20420926]
15. Satpute AB, Wager TD, Cohen-Adad J, Bianciardi M, Choi JK, Buhle JT, Wald LL, Barrett LF. Identification of discrete functional subregions of the human periaqueductal gray. Proc Natl Acad Sci U S A. 2013; 110:17101–6. [PubMed: 24082116]
16. Desikan RS, Segonne F, Fischl B, Quinn BT, Dickerson BC, Blacker D, Buckner RL, Dale AM, Maguire RP, Hyman BT, Albert MS, Killiany RJ. An automated labeling system for subdividing the human cerebral cortex on MRI scans into gyral based regions of interest. Neuroimage. 2006; 31:968–980. [PubMed: 16530430]
17. Diedrichsen J, Balsters JH, Flavell J, Cussans E, Ramnani N. A probabilistic MR atlas of the human cerebellum. Neuroimage. 2009; 46:39–46. [PubMed: 19457380]
18. Bassett DS, Bullmore E. Small-world brain networks. Neuroscientist. 2006; 12:512–523. [PubMed: 17079517]
19. Nioche C, Cabanis EA, Habas C. Functional Connectivity of the Human Red Nucleus in the Brain Resting State at 3T. AJNR Am J Neuroradiol. 2009; 30:396–403. [PubMed: 19022864]
20. Habas C, Cabanis EA. Cortical projection to the human red nucleus: complementary results with probabilistic tractography at 3 T. Neuroradiology. 2007; 49:777–784. [PubMed: 17643241]

21. Jang SH, Chang PH, Kwon HG. The neural connectivity of the inferior olivary nucleus in the human brain: A diffusion tensor tractography study. Neurosci Lett. 2012; 523:67–70. [PubMed: 22743659]
22. Lehericy S, Bardinet E, Poupon C, Vidailhet M, Francois C. 7 Tesla magnetic resonance imaging: a closer look at substantia nigra anatomy in Parkinson's disease. Mov Disord. 2014; 29:1574–1581. [PubMed: 25308960]
23. Yetnikoff L, Lavezzi HN, Reichard RA, Zahm DS. An update on the connections of the ventral mesencephalic dopaminergic complex. Neuroscience. 2014; 282C:23–48. [PubMed: 24735820]
24. Menke RA, Jbabdi S, Miller KL, Matthews PM, Zarei M. Connectivity-based segmentation of the substantia nigra in human and its implications in Parkinson's disease. Neuroimage. 2010; 52:1175–1180. [PubMed: 20677376]
25. Chowdhury R, Lambert C, Dolan RJ, Duzel E. Parcellation of the human substantia nigra based on anatomical connectivity to the striatum. Neuroimage. 2013; 81:191–198. [PubMed: 23684858]
26. Benarroch EE. Subthalamic nucleus and its connections: Anatomic substrate for the network effects of deep brain stimulation. Neurology. 2008; 70:1991–1995. [PubMed: 18490619]
27. Lambert C, Zrinzo L, Nagy Z, Lutti A, Hariz M, Foltynie T, Draganski B, Ashburner J, Frackowiak R. Confirmation of functional zones within the human subthalamic nucleus: patterns of connectivity and sub-parcellation using diffusion weighted imaging. Neuroimage. 2012; 60:83–94. [PubMed: 22173294]
28. Seeley WW, Menon V, Schatzberg AF, Keller J, Glover GH, Kenna H, Reiss AL, Greicius MD. Dissociable Intrinsic Connectivity Networks for Salience Processing and Executive Control. J Neurosci. 2007; 27:2349–2356. [PubMed: 17329432]
29. Habas C, Kamdar N, Nguyen D, Keller K, Beckmann CF, Menon V, Greicius MD. Distinct Cerebellar Contributions to Intrinsic Connectivity Networks. J Neurosci. 2009; 29:8586–8594. [PubMed: 19571149]
30. Paxinos, G.; Huang, X.; Sengul, G.; Watson, C. Organization of brainstem nuclei. In: Mai, JK.; Paxinos, G., editors. The Human Nervous System. 3. Elsevier Academic Press; Amsterdam: 2012. p. 260-327.
31. Vertes, R.; Linley, S. Efferent and afferent connections of the dorsal and median raphe nuclei in the rat. In: Monti, JM.; Pandi-Perumal, SR.; Jacobs, BL.; Nutt, DJ., editors. Serotonin and Sleep: Molecular, Functional and Clinical Aspects. Birkhäuser Verlag; Switzerland: 2008. p. 69-102.
32. Dorocic IP, Furth, Xuan Y, Johansson Y, Pozzi L, Silberberg G, Carlen M, Meletis K. A whole-brain atlas of inputs to serotonergic neurons of the dorsal and median raphe nuclei. Neuron. 2014; 83:663–678. [PubMed: 25102561]
33. Greicius MD, Krasnow B, Reiss AL, Menon V. Functional connectivity in the resting brain: a network analysis of the default mode hypothesis. Proc Natl Acad Sci USA. 2003; 100:253–258. [PubMed: 12506194]
34. O'Reilly JX, Beckmann CF, Tomassini V, Ramnani N, Johansen-Berg H. Distinct and overlapping functional zones in the cerebellum defined by resting state functional connectivity. Cereb Cortex. 2010; 20:953–965. [PubMed: 19684249]
35. Smith SM, Fox PT, Miller KL, Glahn DC, Foc PM, Mackay CE, Filippini N, Watikins KE, Toro R, Laird AR, Beckmann CF. Correspondence of the brain's functional architecture during activation and rest. Proc Natl Acad Sci USA. 2009; 106:13040–13045. [PubMed: 19620724]
36. Beliveau V, Svarer C, Frokjaer VG, Knudsen GM, Greve DN, Fisher PM. Functional connectivity of the dorsal and median raphe nuclei at rest. Neuroimage. 2015; 116:187–195. [PubMed: 25963733]
37. Millan MJ. Descending control of pain. Prog Neurobiol. 2002; 66:355–474. [PubMed: 12034378]
38. Niblock MM, Kinney HC, Luce CJ, Belliveau RA, Filiano JJ. The development of the medullary serotonergic system in the piglet. Auton Neurosci. 2004; 110:65–80. [PubMed: 15046730]
39. Gruber P, Gould DJ. The red nucleus: past, present, and future. Neuroanatomy. 2010; 9:1–3.
40. Beissner F, Schumann A, Brunn F, Eisenträger D, Bär KJ. Advances in functional magnetic resonance imaging of the human brainstem. Neuroimage. 2014; 86:91–98. [PubMed: 23933038]
41. Beissner, F.; Polimeni, JR.; Biancardi, M.; Renvall, V.; Eichner, C.; Napadow, V.; Wald, LL. Imaging the human brainstem at 7 Tesla using multi-modal echo-planar imaging. Proceedings of

the 22nd scientific meeting, International Society for Magnetic Resonance in Medicine; Milan. 2014. p. 1413

42. Bianciardi, M.; Toschi, N.; Eichner, C.; Setsompop, K.; Polimeni, JR.; Rosen, BR.; Wald, LL. Validation of in vivo structural template of human brainstem nuclei by fMRI at 7 Tesla. Proceedings of the 23rd scientific meeting, International Society for Magnetic Resonance in Medicine; Toronto. 2015. p. 272
43. Craddock RC, James GS, Holtzheimer PE 3rd, Hu XP, Mayberg HS. A whole brain fMRI atlas generated via spatially constrained spectral clustering. Human Brain Mapp. 2012; 33:1914–28.
44. Smith SM, Beckmann CF, Andersson J, Auerbach EJ, Bijsterbosch J, Douaud G, Duff E, Feinberg DA, Griffanti L, Harms MP, Kelly M, Laumann T, Miller KL, Moeller S, Petersen S, Power J, Salimi-Khorshidi G, Snyder AZ, Vu AT, Woolrich MW, Xu J, Yacoub E, Ugurbil K, Van Essen DC, Glasser MF. WU-Minn HCP Consortium. Resting-state fMRI in the Human Connectome Project. Neuroimage. 2013; 80:144–68. [PubMed: 23702415]
45. Chen T, Ryali S, Qin S, Menon V. Estimation of resting-state functional connectivity using random subspace based partial correlation: a novel method for reducing global artifacts. Neuroimage. 2013; 82:87–100. [PubMed: 23747287]
46. Bianciardi M, Fukunaga M, van Gelderen P, Horovitz SG, de Zwart JA, Shmueli K, Duyn JH. Sources of functional magnetic resonance imaging signal fluctuations in the human brain at rest: a 7 T study. Magn Reson Imaging. 2009; 27:1019–1029. [PubMed: 19375260]
47. Behrens TE, Johansen-Berg H, Woolrich MW, Smith SM, Wheeler-Kingshott CA, Boulby PA, Barker GJ, Sillery EL, Sheehan K, Ciccarelli O, Thompson AJ, Brady JM, Matthews PM. Non-invasive mapping of connections between human thalamus and cortex using diffusion imaging. Nat Neurosci. 2003; 6:750–757. [PubMed: 12808459]
48. Tziortzi AC, Haber SN, Searle GE, Tsoumpas C, Long CJ, Shotbolt P, Douand G, Jbabdi S, Behrens TE, Rabiner EA, Jenkinson M, Gunn RN. Connectivity-Based Functional Analysis of Dopamine Release in the Striatum Using Diffusion-Weighted MRI and Positron Emission Tomography. Cereb Cortex. 2014; 24:1165–1177. [PubMed: 23283687]
49. Giacino JT, Fins JJ, Laureys S, Schiff ND. Disorders of consciousness after acquired brain injury: the state of the science. Nat Rev Neurol. 2014; 10:99–114. [PubMed: 24468878]
50. Pellicano C, Benincasa D, Pisani V, Buttarelli FR, Giovannelli M, Pontieri FE. Prodromal non-motor symptoms of Parkinson's disease. Neuropsychiatr Dis Treat. 2007; 3:145–152. [PubMed: 19300544]
51. Postuma RB, Aarsland D, Barone P, Burn DJ, Hawkes CH, Oertel W, Ziemssen T. Identifying prodromal Parkinson's disease: pre-motor disorders in Parkinson's disease. Mov Disord. 2012; 27:617–626. [PubMed: 22508280]
52. Irimia A, Chambers MC, Torgerson CM, Filippou M, Hovda DA, Alger JR, Gerig G, Toga AW, Vespa PM, Kikinis R, Van Horn JD. Patient-tailored connectomics visualization for the assessment of white matter atrophy in traumatic brain injury. Front Neurol. 2012b; 3:10.doi: 10.3389/fneur.2012.00010 [PubMed: 22363313]
53. Van Horn JD, Irimia A, Torgerson CM, Chambers MC, Kikinis R, Toga AW. Mapping connectivity damage in the case of Phineas Gage. PLoS One. 2012; 7:e37454.doi: 10.1371/journal.pone.0037454 [PubMed: 22616011]
54. Pandit AS, Robinson E, Aljabar P, Ball G, Gousias IS, Wang Z, Hajnal JV, Rueckert D, Counsell SJ, Montana G, Edwards AD. Whole-brain mapping of structural connectivity in infants reveals altered connection strength associated with growth and preterm birth. Cereb Cortex. 2013; 24:2324–2333. [PubMed: 23547135]
55. Paxinos, G.; Huang, XF. Atlas of the human brainstem. Academic Press; San Diego: 1995.
56. Naidich, TP.; Duvernoy, HM.; Delman, BN.; Sorensen, AG.; Kollias, SS.; Haacke, EM. Duvernoy's atlas of the human brain stem and cerebellum: high-field MRI, surface anatomy, internal structure, vascularization and 3D sectional anatomy. Springer; Wien, New York: 2009.
57. McNab JA, Edlow BL, Witzel T, Huang SY, Bhat H, Heberlein K, Feiweier T, Liu K, Keil B, Cohen-Adad J, Tisdall MD, Folkerth RD, Kinney HC, Wald LL. The Human Connectome Project and beyond: initial applications of 300 mT/m gradients. Neuroimage. 2013; 80:234–245. [PubMed: 23711537]

58. Destrieux C, Fischl B, Dale A, Halgren E. Automatic parcellation of human cortical gyri and sulci using standard anatomical nomenclature. Neuroimage. 2010; 53:1–15. [PubMed: 20547229]

59. Desikan RS, Segonne F, Fischl B, Quinn BT, Dickerson BC, Blacker D, Buckner RL, Dale AM, Maguire RP, Hyman BT, Albert MS, Killiany RJ. An automated labeling system for subdividing the human cerebral cortex on MRI scans into gyral based regions of interest. Neuroimage. 2006; 31:968–980. [PubMed: 16530430]

60. Tzourio-Mazoyer N, Landeau B, Papathanassiou D, Crivello F, Etard O, Delcroix N, Mazoyer B, Joliot M. Automated anatomical labeling of activations in SPM using a macroscopic anatomical parcellation of the MNI MRI single-subject brain. Neuroimage. 2002; 15:273–289. [PubMed: 11771995]

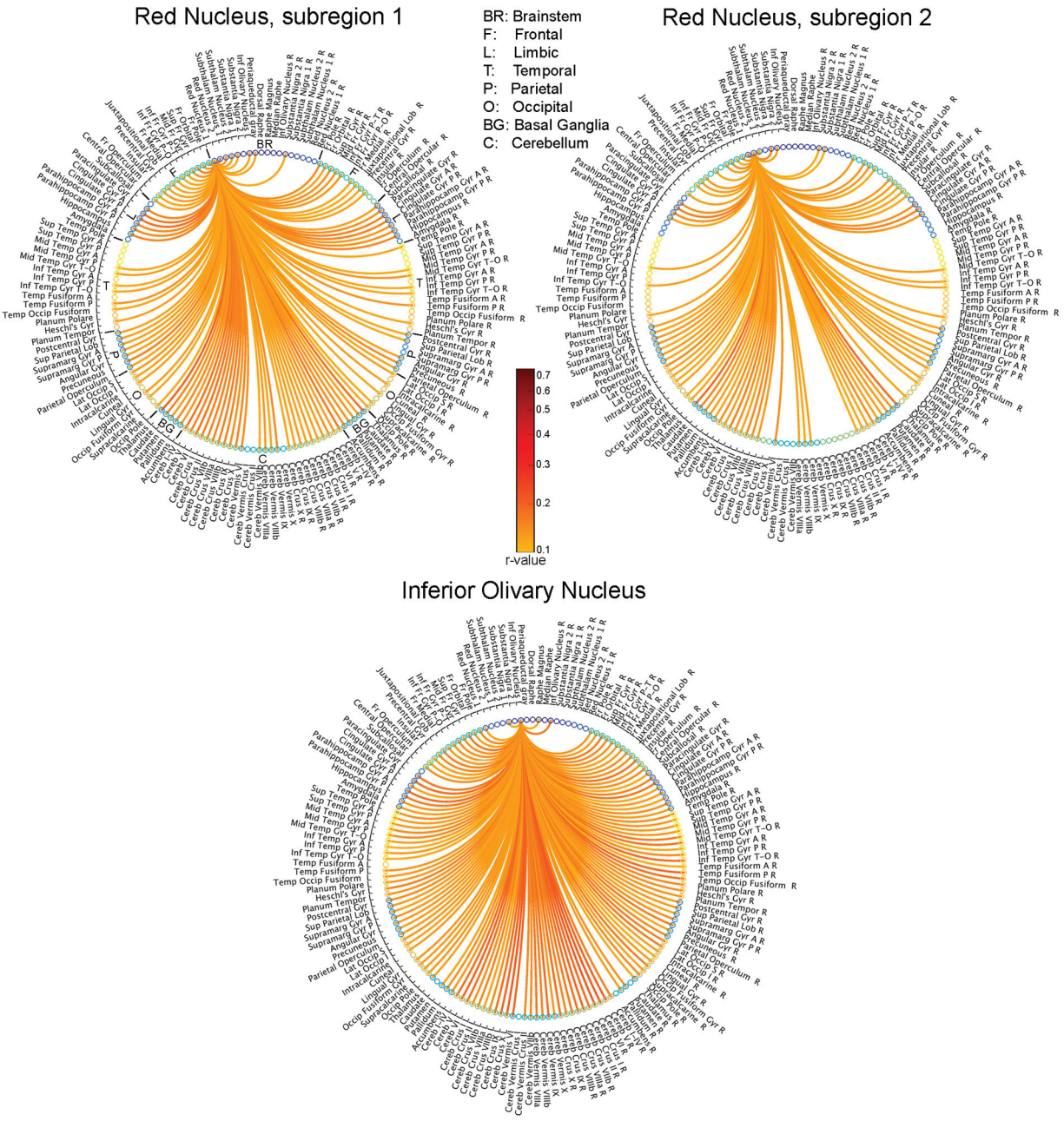

Figure 1. Functional connectome of two subregions of the red nucleus and of the inferior olivary nucleus (rubro-olivary-cerebellar motor network)

Significant ($q < 0.05$, false discovery rate, FDR, group level, n = 12) Pearson's correlation (r) values between signals of three seed Bn (left subregion 1 and subregion 2of red nucleus, —indicated as Red Nucleus 1 and 2, left inferior olivary nucleus) and 155 target brain regions (including 17 Bn other than the seed) are displayed as links between seed and target regions. Abbreviations used: L/R = left/right; Inf/Sup/Mid/Lat = inferior/superior/middle/lateral; A/P = anterior/posterior; Fr/Temp/Occip = frontal/temporal/occipital; Lob = lobule; Gyr = gyrus; P-T/P-O = pars triangularis/pars opercularis; Tempor = temporal; T-O = temporo-occipital; Cereb = cerebellum; Supramarg = supramarginal; Subthalam =

subthalamic. Note that the color scheme of the small circles displayed for each region in Figures 1–3 is arbitrary, and does not encode for any connectivity measure.

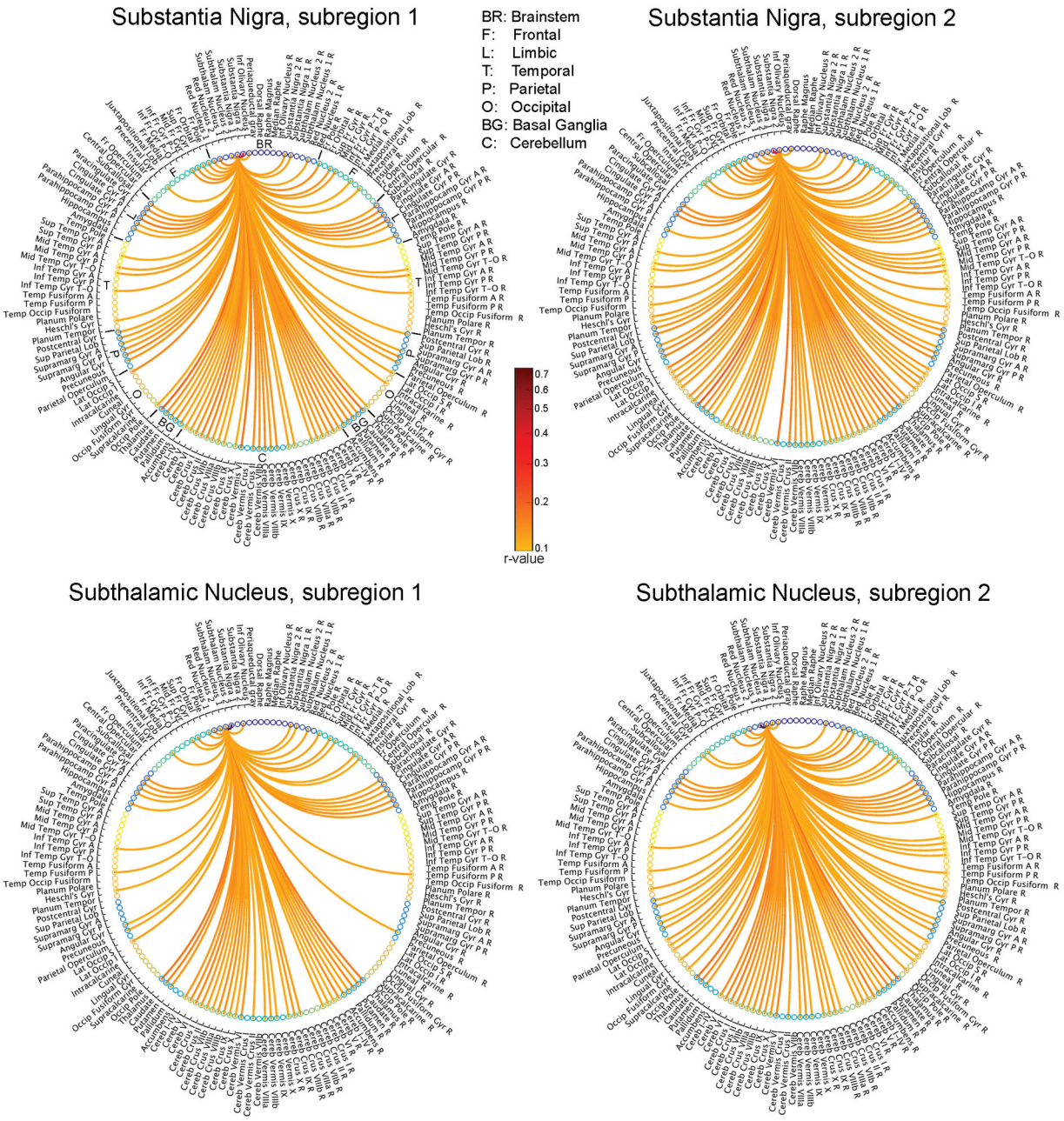

Figure 2. Functional connectome of two subregions of the substantia nigra and of the subthalamic nucleus (nigro-subthalamic-basal ganglia motor network)

Significant ($q < 0.05$, false discovery rate, FDR, group level, n =12) Pearson's correlation (r) values between signals of four seed Bn (left subregion 1 and subregion 2 of substantia nigra–indicated as Substantia Nigra 1 and 2, left subregion 1 and subregion 2 of subthalamic nucleus–indicated as Subthalam Nucleus 1 and 2) and 155 target brain regions (including 17 Bn other than the seed) are displayed as links between seed and target regions.

Abbreviations used: L/R = left/right; Inf/Sup/Mid/Lat = inferior/superior/middle/lateral; A/P = anterior/posterior; Fr/Temp/Occip = frontal/temporal/occipital; Lob = lobule; Gyr = gyrus;

P-T/P-O = pars triangularis/pars opercularis; Tempor = temporal; T-O = temporo-occipital; Cereb = cerebellum; Supramarg = supramarginal; Subthalam = subthalamic.

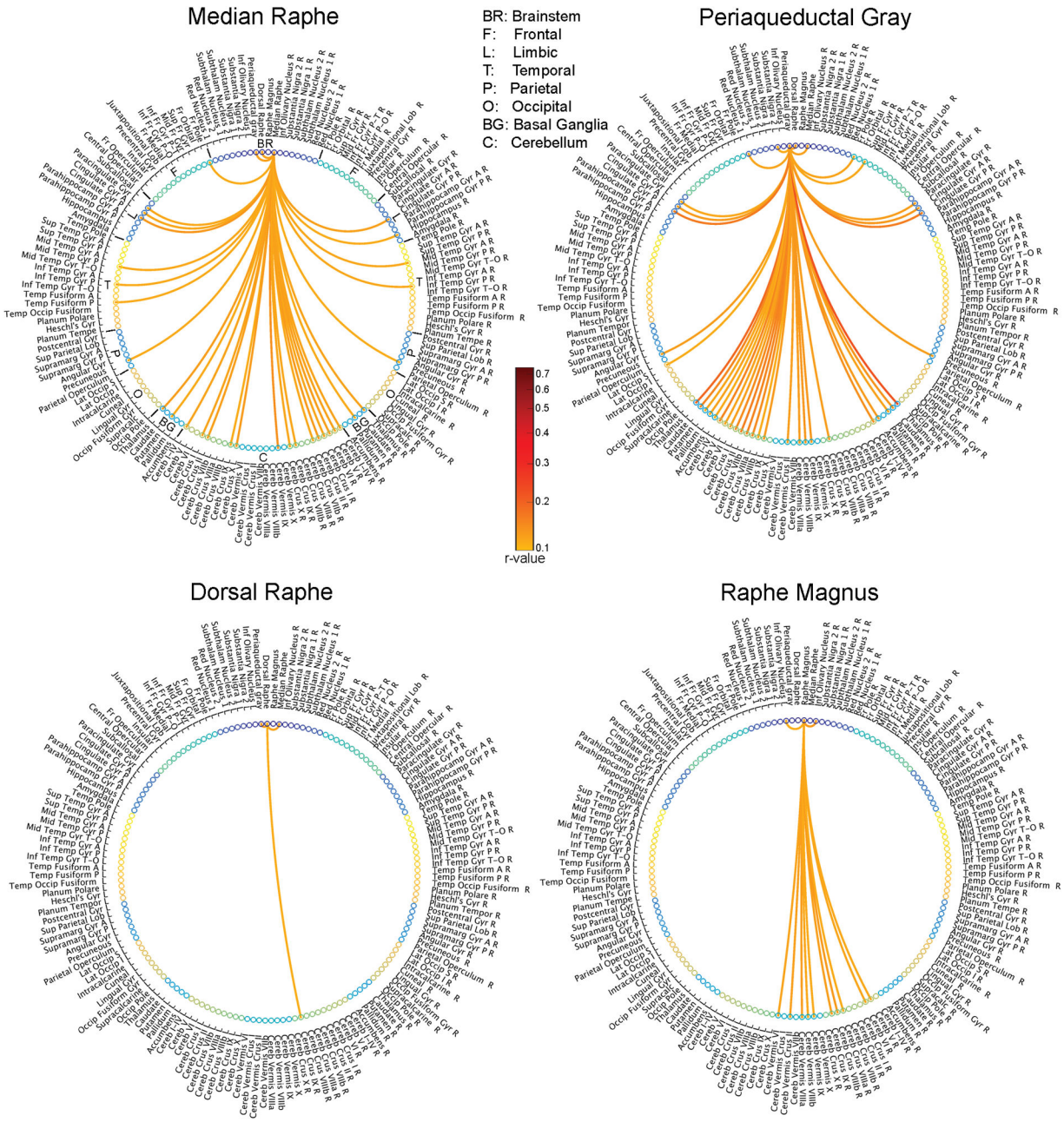

Figure 3. Functional connectome of the median raphe, dorsal raphe, periaqueductal gray and raphe magnus (ascending arousal/autonomic network)

Significant ($q < 0.05$, false discovery rate, FDR, group level, n =12) Pearson's correlation (r) values between signals of four seed Bn (median raphe, dorsal raphe, periaqueductal gray and raphe magnus) and 155 target brain regions (including 17 Bn other than the seed) are displayed as links between seed and target regions. Abbreviations used: L/R = left/right; Inf/Sup/Mid/Lat = inferior/superior/middle/lateral; A/P = anterior/posterior; Fr/Temp/Occip = frontal/temporal/occipital; Lob = lobule; Gyr = gyrus; P-T/P-O = pars triangularis/pars opercularis; Tempor = temporal; T-O = temporo-occipital; Cereb = cerebellum; Supramarg = supramarginal; Subthalam = subthalamic.

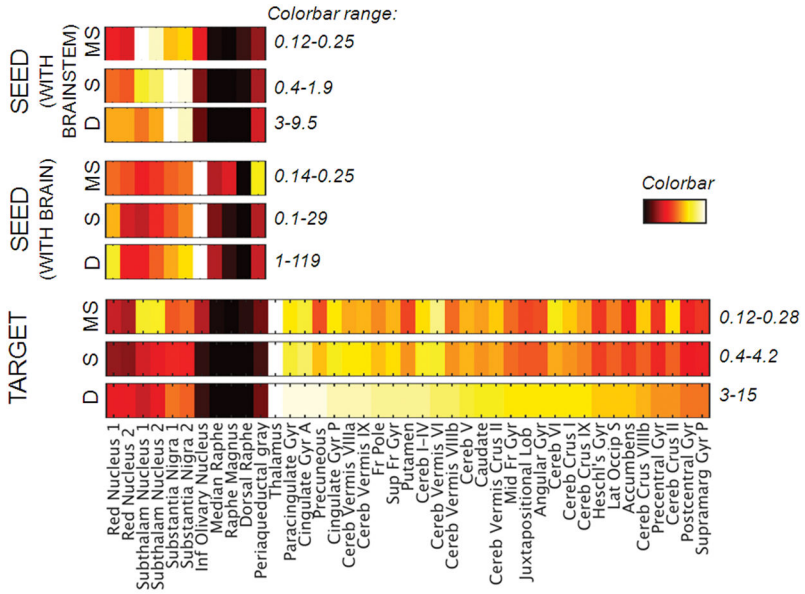

Figure 4. Connectivity metrics of the brainstem-brain connectome

We display: bottom rows (“Target”)) the target-node degree (D), strength (S) and mean-strength (MS) of the 11 investigated Bn (considered as target regions), as well as of the 30 target regions (“hubs”) in the brain (other than Bn) with the highest (all above the average) target-node degree of connectivity with Bn (the target brain hubs are sorted on the basis of their degree); middle rows (“Seed with brain”)) the seed-node degree, strength and mean-strength of Bn towards the brain (excluding Bn), evaluating distal Bn connectivity; top rows (“Seed with brainstem”)) the seed-node degree, strength and mean-strength of Bn towards Bn, evaluating local Bn connectivity. Note that, among target nodes, the thalamus, regions of the limbic system (e.g. paracingulate gyrus, anterior division of the cingulate gyrus), default mode network (e.g. precuneous, posterior division of the cingulated gyrus), executive network (e.g. frontal pole, superior frontal gyrus), cerebellum (e.g. Vermis VIIIa, Vermis IX, I–IV), basal ganglia (putamen, caudate), and sensory-motor networks (e.g. juxtapositional lobule, Heschl’s gyrus, lateral lccipital, precentral and postcentral gyrus) displayed the highest connectivity with Bn. Among seed regions, the inferior olivary nucleus showed the highest distal (brainstem-brain) connectivity, and the two subregions of the substantia nigra the highest local (brainstem-brainstem) connectivity.